Journal of Techniques, ISSN: 2708-8383, Vol. 5, No. 3, 2023, Pages 129-137
DOI: https://doi.org/10.51173/jt.v5i3.1060

JOURNAL OF TECHNIQUES

Journal homepage: http://journal.mtu.edu.iq

RESEARCH ARTICLE - ENGINEERING

Computed Tomography Image Segmentation of Lung Corona Virus Infection Region Based on Combination of Grayscale Morphological Reconstruction and Fast Marching Method

Aws Alazawi[1], Abbas Fadhal Humadi[1], Huda Farooq Jameel[1*], Huda Ali Hashim[1], John Soraghan[2]

[1] Electrical Engineering Technical College, Middle Technical University, Baghdad, Iraq

[2] Centre for Signal and Image Processing, Institute for Sensors, Signals & Communications, Department of Electronic and Electrical Engineering, University of Strathclyde, Glasgow, UK

[*] Corresponding author E-mail: huda_baban@mtu.edu.iq

Article Info.

Article history:

Received
06 November 2022

Accepted
08 January 2023

Publishing
30 September 2023

Abstract

Recently, X-ray computed tomography-imaging modality is considered as golden standard for diagnosis of coronavirus lungs infection. In worldwide, infectious patients increase rapidly that lead to weariness in health services staff, as well as instant treatment required to avoid patients' health deterioration due to infection development. Image processing would be reinforcing health services by considering computer-based segmentation. However, a ground glass computed tomography image fashion of coronavirus lungs infection characterized by disappearance of edge region of interest and lack of object structure. In this study, these challenges addressed by introducing a new algorithm that combined both morphological reconstruction and fast marching method. The proposed algorithm applied on archived computed tomography dataset for coronavirus infected patients, results showed consistent determination of ground glass infection region compared to manual delineation of senior physician. The proposed algorithm restricted to empirical adjustment of FMM's threshold that would be addressed in upcoming study.

Publisher: Middle Technical University

Keywords: Covid-19 Infection; CT Imaging; Fast Marching Method; Gray-Scale Morphological Reconstruction; Medical Image Segmentation.

1. Introduction

COVID-19 is a virus caused by SARS-CoV-2 that can cause mild to severe infections in people. COVID-19 is a disease that has spread around the world. The epidemic has spread fast around the world after its initial appearance in China in December 2019. Despite significant attempts to limit the disease, the virus has persisted in numerous nations with various degrees of clinical presentation. There are many analytical methods available for SARS-CoV-2 detection. Like swap by its RNA, blood with Ag/Ab and chest X-ray Computed Tomography (CT) as well as X-ray image [1].

Subpleural distribution was detected in the normal CT findings of bilateral ground-glass opacities and consolidation. The additional pulmonary consolidation observed on CT, the more likely it was that the initial reverse transcription – polymerase chain reaction findings would be negative. Repeated Reverse Transcription-Polymerase Chain Reaction (RT-PCR) testing and patient isolation should be explored in patients with suspected COVID-19 pneumonia who have an epidemiologic history and whose CT findings are virtuous [2]. One major disadvantage of using RT-PCR to diagnose COVID-19 is that it can provide false-negative results, especially in the early stages of infection, so CT scans are best for diagnosing COVID-19.

Medical imaging, such as X-ray and CT, considered as medical imaging modality for COVID-19, while newly emerging Artificial Intelligence (AI) technologies enhance the power of imaging tools and assist medical professionals. Several studies have revealed how AI as accurate, and efficient imaging solutions in COVID-19 applications [3], including intelligent imaging platforms, clinical diagnostics, and pioneering research. As a result, it is critical to integrate imaging data with clinical symptoms and laboratory examination results to aid in the screening, identification, and diagnosis of COVID-19. In this case, AI exhibits inherent capacity to fuse information from several sources to perform accurate and efficient diagnosis, analysis, and follow-up. An X-and Y-attention module introduced that could improve lung segmentation performance on chest X-ray images by emphasizing features, which was made up of channel and spatial attention, allows for the effective extraction of global and local characteristics [4]. However, chest X-rays with malformed lungs or an unclear cardiac profile demonstrated poor lung segmentation performance, which warrants further investigation.

Nomenclature & Symbols			
AI	Artificial Intelligence	DPSO	Dynamic Particle Swarm Optimization
CT	Computed Tomography	N.A.	Not Available
CNN	Convolutional Neural Network	TB	Tuberculosis
DCN	Dual-Branch Combination Network	NIfTI	Neuroimaging Informatics Technology Initiative
RT-PCR	Reverse Transcription- Polymerase Chain Reaction	δ	Morphological Dilation of Marker G by a Flat Structuring Element of B
DBSCAN	Density-Based Spatial Clustering of Applications with Noise	ε	Morphological Erosion of Marker G by a Flat Structuring Element of B
SUFMACS	Super Pixel-Based Fuzzy Memetic Advanced Cuckoo Search	D-, D+	Backward and Forward Difference Operators Respectively
GGOs	Ground-Glass Opacities	t	Evolution Time
FCM	Fuzzy C-Means	φ_t	Curve's Movement
FEMO	Fuzzy Electromagnetism Optimization	∇φ	Evolution Curve
GAN	Generative Adversarial Network	F	Normal Direction Speed of Evolution that Related to the Image Nature
SLDT	Stacked Loopy Decision Tree		

Chest radiography of X-ray was the most frequent diagnostic approach for pulmonary diseases, many researchers utilized to examine chest radiography, their research focused on publicly available datasets employing chest X-rays for lung segmentation and the detection as well as classification of pulmonary diseases [5]. The investigations were carried out on chest X-rays utilizing the Generative Adversarial Network (GAN) models for segmentation and classification. From that end, a two-stage generative adversarial network proposed. The suggested method uses a GAN to build a synthesized binary mask, and then developed by including the second GAN to conduct conditional production of image synthesis [6]. GAN is used to create synthetic image-mask, which were then utilized to enhance the performance of traditional image segmentation algorithms. Generally, researches were performed prior to the popularity of deep learning models to provide a complete view of the field. A taxonomy of state-of-the-art deep learning-based lung disease detection systems was suggested [7], to visualize the trends of recent work in the area and identify the remaining challenges and potential future paths in this domain. A combination of both modern CT imaging and virtual reality technologies introduced to create an automated method for screening the condition, where the combined system potentially utilized for medical education and professional training as a telemedicine virtual reality platform [8].

The automated identification of lung infections using CT images can substantially supplement the standard healthcare strategy for the determination of COVID-19. However, segmenting infected areas from CT slices is a challenge due to considerable diversity in infection features and poor intensity contrast between infections and normal tissues. A novel COVID-19 lung infection segmentation technique of deep network was presented to detect infection region automatically [9]. A semi-supervised framework is used to improve learning abilities and producing considerable results, where a segmentation technique based on a fuzzy algorithm suggested by considering an enhanced clustering approach, both sub-graph decomposition and area merging were utilized to improve the clustering of the fuzzy C-mean segmentation algorithm, the findings demonstrated that the technique was good ingot results [10].

However, the edge of a CT imaging lesion is generally affected by pixels with uneven grey-scale and isolated noise, making weak edge identification of the COVID-19 lesion as a challenge. To address this issue, an edge detection approach that combines histogram equalization with the enhanced canny algorithm was presented [11]. The experimental findings showed that the suggested method could detect the weak edge of the lesion, and useful for COVID-19 diagnosis. In the same way, a PointNet++ and AI-driven unsupervised machine learning technique used to detect and Quantify Ground-Glass Opacities (GGOs) in CT scans of COVID-19 patients [12]. This method identified GGOs with the greatest evaluation accuracy (98%), average class correctness (95%), and intersection over union (92%). Furthermore, a unique technique based on a Stacked Loopy Decision Tree (SLDT) introduced for label prediction in traditional tree-based image analysis models [13]. Stacked decision trees could help with medical image analysis, such as image screening and Tuberculosis (TB) classification. For a clinical imaging application, SLDT can offer a good choice tree model with an integrated stacking encoder. Moreover, , a novel unsupervised machine learning-based algorithm of Super pixel-based Fuzzy Memetic Advanced Cuckoo Search (SUFMACS) presented to efficiently analysis and segment the COVID-19 radiological pictures [14]. This method extends the super pixel method to decrease a large amount of spatial information. Furthermore, a hybrid segmentation strategy proposed that based on an improved fuzzy c-means clustering algorithm that combined with the level set for lung segmentation [15]. The suggested technique performance examined using two public chest x-ray datasets: JRST and Montgomery County. However, optimization approaches could be used to enhance the findings, and required to evaluate the performance of various lung segmentation algorithms with datasets of varying sizes. Further exemplified in studies is a lung segmentation that accomplished using a relationship between the segmentation mask generator network and the discriminator network, this technique could distinguish between the right mask and the created mask [16].

Further studies considered computer-aided technique to identify early symptoms of COVID-19 infection from CT scan images, super pixel based fuzzy modified flower pollination algorithm technique introduced to employ the idea of the super pixel to efficiently analysis the spatial information of CT scans that could aid in early isolation and treatment [17]. A novel unsupervised classification technique using Fuzzy Electromagnetism Optimization (FEMO) suggested where efficiency improved in FEMO by integrating with the modified type 2 fuzzy C-Means algorithm [18]. Meanwhile, to reduce the effect of intensity changes across CT slices, pre-processing performed, where Long Short-Term Memory (LSTM) neural network classifier used to classify the collected characteristics, the greatest accuracy attained for categorizing the gathered dataset of 321 patients was 99.68% [19].

Medical image segmentation is an active research area, where focused Tversky loss technique introduced for segmentation of a local patch lesion. Dataset of 100 CT slices conducted in the study that demonstrating an accurate and rapid COVID-19 segmentation represented by quantitative measurement of dice account of 83.1% [20]. On the other hand, a Dual-Branch Combination Network (DCN) for COVID-19 diagnosis established, where a slice probability approach presented to learn the translation from slice-level for individual-level. The findings showed that the proposed DCN achieves an accuracy of 96.74% [21]. Additionally, a Convolutional Neural Network (CNN) model to separate lung parenchyma using a clustering algorithm-based solution was presented [22]. A contour detection challenge and novel image processing

method was established, where many impacted and non-influenced images acquired from an internet knowledge source tested against the proposed framework [23]. Recently, researchers investigated a variety of approaches in medical image processing. Such as a hybrid technique, combining Dynamic Particle Swarm Optimization (DPSO) and fuzzy C-means (FCM) with a noise reduction mechanism was presented [24].

In segmentation of non-existence of non-structuring object, as a retinal blood vessels in healthcare photographs considered a combining morphological reconstruction with integrated segmentation, where patterns generated utilizing Density-Based Spatial Clustering of Applications with Noise (DBSCAN). Images with more veins were first stripped-down, followed by pruning. This technique restored a lost thin vasculature and identified a number of fresh thin vessels not depicted in the ground truth. Consequently, the algorithm performs better and a more thorough pattern was produced. However, using clustered pixels in the image's sloped management, this approach could be improved [25]. On the other hand, a pothole classification method was presented to detect non-existence of edge in a road image, where computation issue addressed. The computing issue simplified accordingly, where the suggested technique transforms RGB image information to a grayscale, by including potholes and other objects. Using an object detection technique, it can identify anything but potholes. The hole from the account of the views considered to determine the real size, where the research should extract certain characteristics from the hole [26]. A quick and effective method proposed for detecting the early signs of Alzheimer's disease using image analysis to detect the non-existence of edges. The prototype includes expansion, and widely applied to identify various neurological illnesses [27]. Image segmentation has been enhanced in some way by all the aforementioned techniques.

The related studies in the literature has been classified according to segmentation techniques as illustrated in Table 1, where highest accuracy was 99.68%, sensitivity was 98.77%, and specify was 97.3% that can be considered as comparison criteria. Furthermore, the drawback from the related work that some of the research has false negative results especially in the early stage of infections. From this points based contrast variation and non-structuring region of interest that motivated researchers to introduce their methodologies as proposed approaches.

In this study, the contribution represents segmentation of lungs infection region that characterized by non-existence of edge and non-structuring object, where the segmentation algorithm combines grayscale morphological reconstruction technique for converting ground-glass region into flat patches and fast marching method for regional growing. The rest of the study arranged into section two as a background that describes proposed segmentation algorithm in terms of mathematical representation, while section three resume methodology by considering algorithm flowchart, finally results and discussion introduced in section four, and conclusion in section five.

Table 1. Comparison of related studies

Reff./year	Segmentation approach	Segmentation results	Objectives
[7]2020	Dual-branch combination network	96.74% (accuracy)	Integrate the intermediate segmentation
[10]2020	Deep network (Inf-Net)	73.9% (dice) 72.5% (sensitivity) 96% (specificity)	To detect poor infected area chest CT slices image
[11]2018	Fuzzy	N.A.	Improve fuzzy clustering algorithm for image segmentation
[13]2021	PointNet++	95% (accuracy)	Detect and quantify GGO in CT scan
[14]2021	SLDT method	98.96% (accuracy) 98.77% (sensitivity) 97.3% (specificity)	SLDT could be accurately predicted in CXR according to the various datasets
[15]2021	SUFMACS	N.A.	Helping the physicians in easy interpretation of the chest CT
[20]2020	Long short term memory neural network	99.68% (accuracy)	Reduce the effect of intensity variations between CT scans
[21]2020	U-Net network	83.1% (dice)	Improve the small ROI segmentation performance

2. Background

The grayscale X-ray CT images include seeded features of Covid-19 infection, features have been considered as regional maxima to be converted into flat patches using morphological reconstruction as pre-operation step toward image segmentation. In grayscale, morphological reconstruction, marker and mask images have to be defined first to determine the starting point and constrain of the conversion respectively.

An elementary geodesic dilation and erosion are mathematically represented as [28, 29]:

$$\begin{cases} R_I^{\delta}(G) = \delta_I^n(G), \ where \quad \delta_I^{n=1}(G) = (G \oplus B) \wedge I \quad for \quad G \leq I \\ R_I^{\varepsilon}(G) = \varepsilon_I^n(G), \ where \quad \varepsilon_I^{n=1}(G) = (G \ominus B) \vee I \quad for \quad G \geq I \end{cases} \tag{1}$$

To determine the morphological reconstruction of grayscale image of m-bits, the n-times (n=2m) grayscale geodesic dilation and erosion are repeated, as follows [28, 29]:

$$\delta_I^n(G) = \delta_I^1(G)\left(\underbrace{\delta_I^1(G)\left(\delta_I^1(G)\left(\delta_I^1(G)\left(\delta_I^1(G) \ldots \left(\delta_I^1(G)\right)\right)\right)\right)}_{n\text{-}times}\right) \tag{2}$$

$$\varepsilon_I^n(G) = \varepsilon_I^1(G)\left(\underbrace{\varepsilon_I^1(G)\left(\varepsilon_I^1(G)\left(\varepsilon_I^1(G)\left(\varepsilon_I^1(G) \ldots \left(\varepsilon_I^1(G)\right)\right)\right)\right)}_{n\text{-}times}\right) \tag{3}$$

Then the grayscale reconstruction ρ_G (I) is determined by iterating the geodesic dilations and erosions for stability to be reached [28, 29].

$$\rho_G(I) = \lim_{n\to\infty} \delta_I^n(G) \tag{4}$$

$$\rho_G(I) = \lim_{n\to\infty} \varepsilon_I^n(G) \tag{5}$$

In addition, the mathematical representation of compositional morphological opening (R_I^{γ}) and closing (R_I^{ϕ}) reconstructions are as follows [30, 31];

$$\begin{cases} R_I^{\gamma}(G) = R_I^{\delta}\left(R_I^{\varepsilon}(G)\right) \\ R_I^{\phi}(G) = R_I^{\varepsilon}\left(R_I^{\delta}(G)\right) \end{cases} \tag{6}$$

Typical morphological opening is erosion succeeded by dilation, while opening by reconstruction is erosion succeeded by morphological reconstruction. For CT image segmentation, grayscale morphological reconstruction applied by considering sequential operations of opening by reconstruction followed by closing by reconstruction. The first step represents opening by reconstruction, where erosion operation applied, to extract the marker image at disk flat structuring element, using grayscale input image (mask image). Reconstruction operation then performed at four connected neighbors, to determine regional maxima of the seeded features. The second step represents dilation of previously reconstructed image (as mask image) to extract marker image again using same structuring element, and finally reconstruction repeated for the complement of both recent marker and mask images. The second step of morphological reconstruction considered to flattening the regional maxima in form of connected patches.

As regional maxima of infection regions are converted to flat patches, segmentation operation has to be performed by manually mark initial patch region of interest, where final contour converges according to a level set method.

Level set method describes surface that used for evolving zero level set embedded in a higher dimensional function φ(x, t) [30, 31];

$$\varphi(x,t) = \varphi_t + F|\nabla\varphi| \tag{7}$$

For efficient evolution, fast marching algorithm introduced, which starts from a given seed point selected manually or pre-estimated from surrounding region at similar characteristics. The flat patches that already been determined by morphological reconstruction would be segmented by considering surface moving with speed F(x, y)>0, and T(x, y) as a time of crossing the surface to the given point (x, y) that satisfied the following relation [30, 31];

$$F|\nabla T| = 1 \tag{8}$$

When the speed is function of only position, the equation known as "Eikonal" that solved numerically by fast marching method. For flat patched CT image, two-dimensional approximation of the "Eikonal", solution dedicated by considering the following quadrature equation [30, 31];

$$F_{ij=}\left[max\left(D_{ij}^{-x}T, D_{ij}^{+x}T, 0\right)^2 + max\left(D_{ij}^{-y}T, D_{ij}^{+y}T, 0\right)^2\right]^{-0.5} \tag{9}$$

At flat patch regions, evolution surface has to be terminated at interface region. The termination criteria rely into speed decreasing function F(x, y) that based one image local gradient |∇I(x, y)| as follows [30, 31];

$$F(x, y) = 1/(1+\alpha|\nabla(G_\sigma * I(x, y))|), \quad \text{where } \alpha \text{ is constant}>0 \tag{10}$$

and

$$F(x,y) = e^{-\alpha|\nabla(G_\sigma * I(x,y))|} \tag{11}$$

The expression of Gσ*I(x, y) represents a convolution of the image and the Gaussian filter with a standard deviation of σ.

In equation (11), the term of gradient ∇ (Gσ *I(x, y)) approach to zero over the flat patch morphologically reconstructed regions, and accordingly the surface evolved at unity speed F(x, y). As the image gradient intensity rapidly changed, it can be considered as collapsing in flatness. While collapsing begins, the term ∇ (Gσ *I(x, y)) become large and the speed will be close to zero that forces surface evolution to be terminated.

For efficient evolution, fast marching algorithm has considered for so-called Hamilton Jacobi [30, 31];

$$\varphi_t = v|\nabla\emptyset| \tag{12}$$

3. Methodology

The proposed algorithm represented by a flowchart shown in Fig. 1, where input image dimension was 512-by-512, and the database formatted as Neuroimaging Informatics Technology Initiative (NIfTI). using data from The Cancer Imaging Archive (TCIA) [32]. The NIfTI image data converted into grayscale image data. The intensity of grayscale image data adjusted to increase contrast of regional maxima at infected regions. The image contrast enhancement reinforces morphological operations of flat patch conversion. The flat patch conversion performed by morphological reconstruction operations of opening by reconstruction followed by closing by reconstruction. For both reconstruction operations, flat disk structuring element at radius twenty pixels and four connected neighbours were considered. In opening by reconstruction, the marker extracted from input image by erosion operation at given structuring element. The reconstruction then applied using both extracted marker image and a mask (input image), to determine regional maxima of the seeded features. The closing by reconstruction then applied by considering the mask as complement of currently reconstructed image and the complement of marker image that created by dilation operation of input image using same structuring element. The flat patches have obtained as a resultant of sequential operations of both morphological reconstructions.

Semi-automatic segmentation initialized by manually select seed point (value of pixel) located in a specific flat patch region of the reconstructed image. The pixel locations are then considered as a reference to utilize their grayscale value for computing absolute value of the difference between the intensity of each pixel and the reference pixel. An inverse relation is then determined between the absolute difference values and weight matrix, where the large weights represent the small absolute differences, while small weights represent large absolute differences. The segmentation of fast marching method is applied by considering the weight matrix and the spatial parameters of selected seed point according to equations (8-12), where threshold empirically specified. Finally, the infected region localized, then highlighted on grayscale CT image.

4. Results and Discussion

According to the methodology presented in Fig. 1, grayscale intensity adjusted to increase the contrast of regional maxima, where the ground glass of the infection region was prominently manifest, as shown in Fig. 2(a and b). Fig. 2(c and d) showed the histogram of before and after intensity adjusted, where the range of grayscale intensity expanded over the pixels.

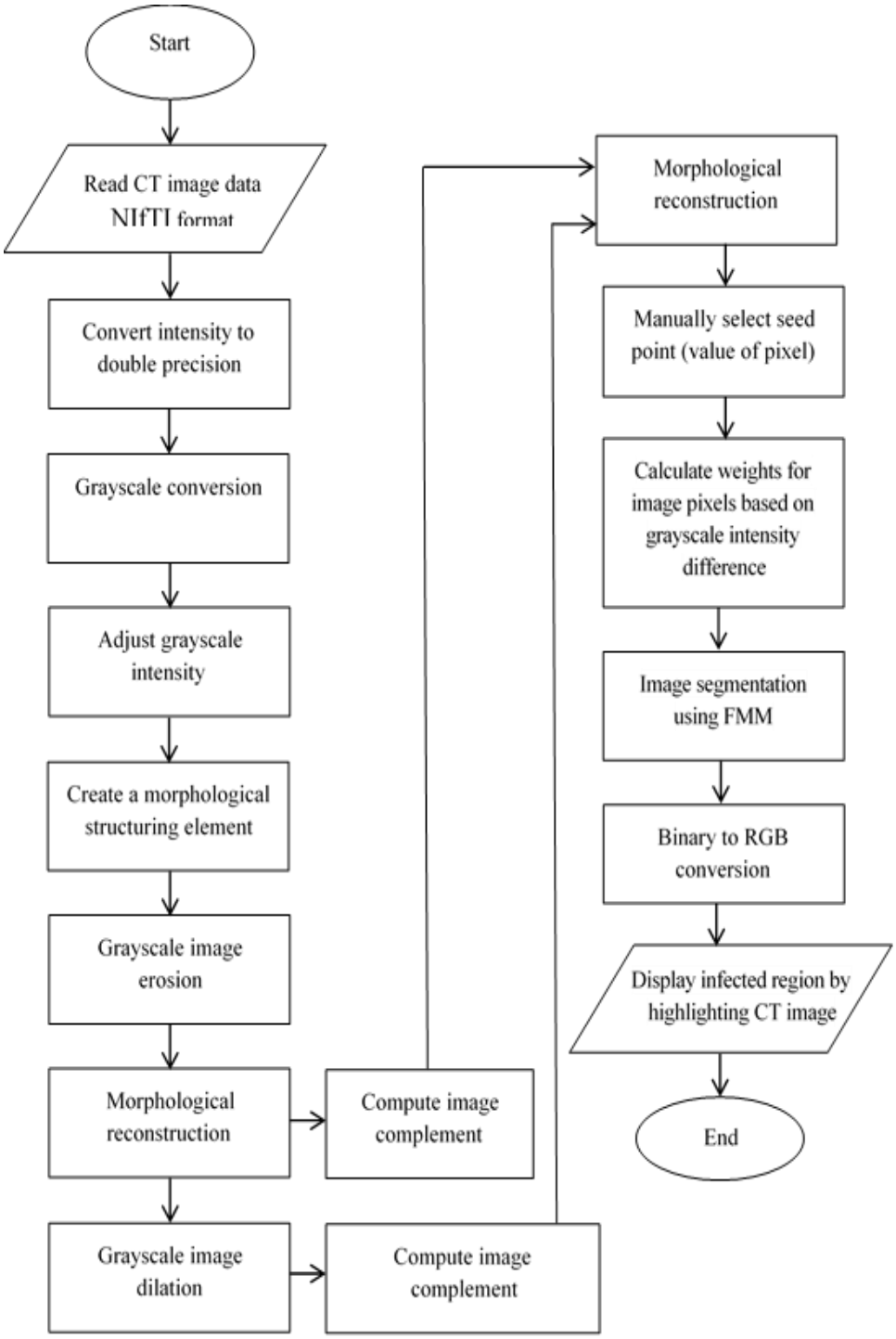

Fig. 1. Flowchart of the proposed algorithm

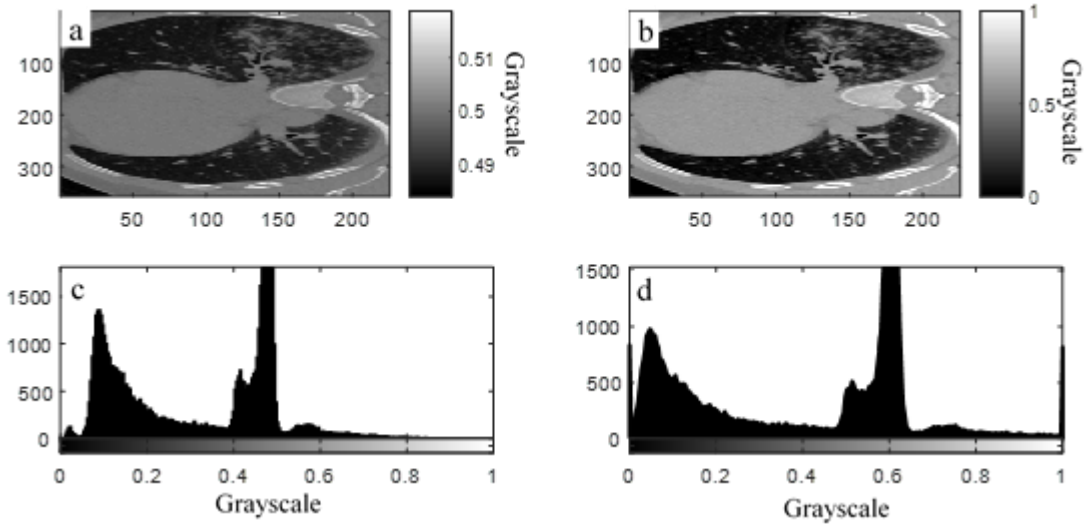

Fig. 2. Grayscale CT, (a) acquired image, (b) intensity adjusted image, (c) histogram of acquired image, (d) histogram of intensity adjusted image

The structuring element created to apply morphological reconstruction operations of opening and closing, where Fig. 3(a and b) showed how the ground glass of infected region shown in Fig. 2(b) converted into flat patches as a result of opening by reconstruction shown in Fig. 3(a) and closing by reconstruction shown in Fig. 3(b) operations respectively.

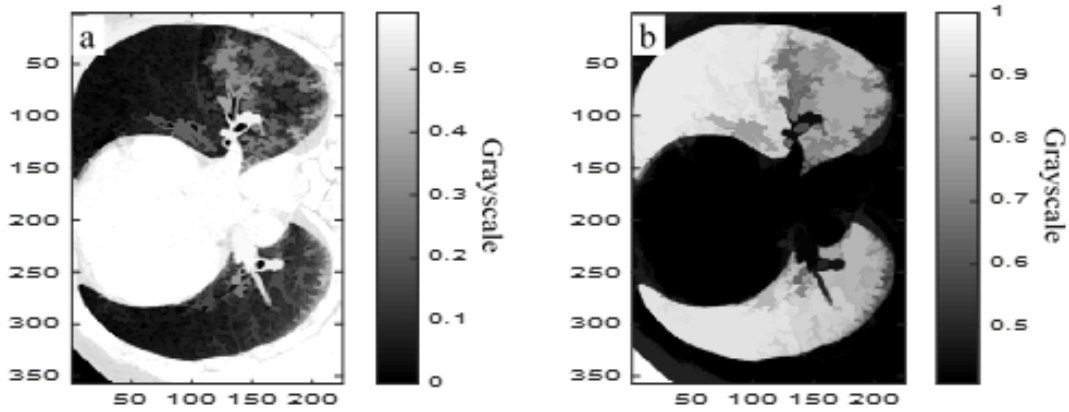

Fig. 3. (a) opening by reconstruction flat patch converted image, (b) closing by reconstruction flat patch converted image

The start point is manually selected from the largest flat patch as shown in Fig. 4(a), where the grayscale intensity of the selected pixel of interest will be considered as an input to the algorithm step of weights calculation that based on intensity difference as shown in Fig. 4(b). The matrix of the weights is in a same size of input image, where the weight represents the reciprocal of absolute intensity difference. As a result, pixels intensities closed from reference intensity would be in small differences, where their weights would be large and represented by white patch shown in Fig. 4(b).

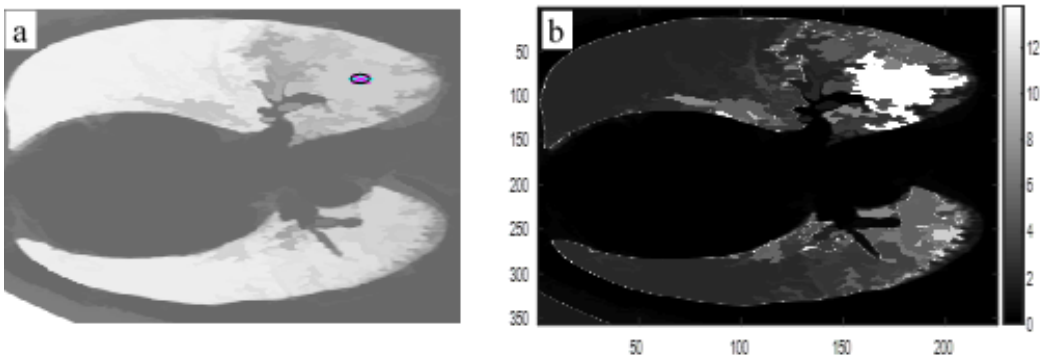

Fig. 4. (a) Start point selection from largest flat patch pointed by black circle, (b) weight calculation regions based on grayscale intensity difference

The segmentation operation of FMM applied to separate regions according to efficient evolution as in equations (7-12). The FMM operation produced geodesic distance map that normalized as shown in Fig. 5(a). The binary image of foreground and background regions formed according to pixels of geodesic distance greater or less than specified threshold that empirically determined, then the binary image converted to RGB as shown in Fig. 5(b). Both RGB image of infection region and CT grayscale lungs image superimposed as shown Fig. 5(c), where the FMM segmentation is consistent with physician delineated infection region as shown in Fig. 5(d).

Further patient analysis infection region has also considered as shown in Fig. 6 and 7, where the image intensity adjustment has effectively superimposed the grayscale intensity over the entire image space as shown in Fig. 6(a-d). The proposed algorithm has considerably determined the infection region, which is consistent with physician delineation as shown in Fig. 7(a and b).

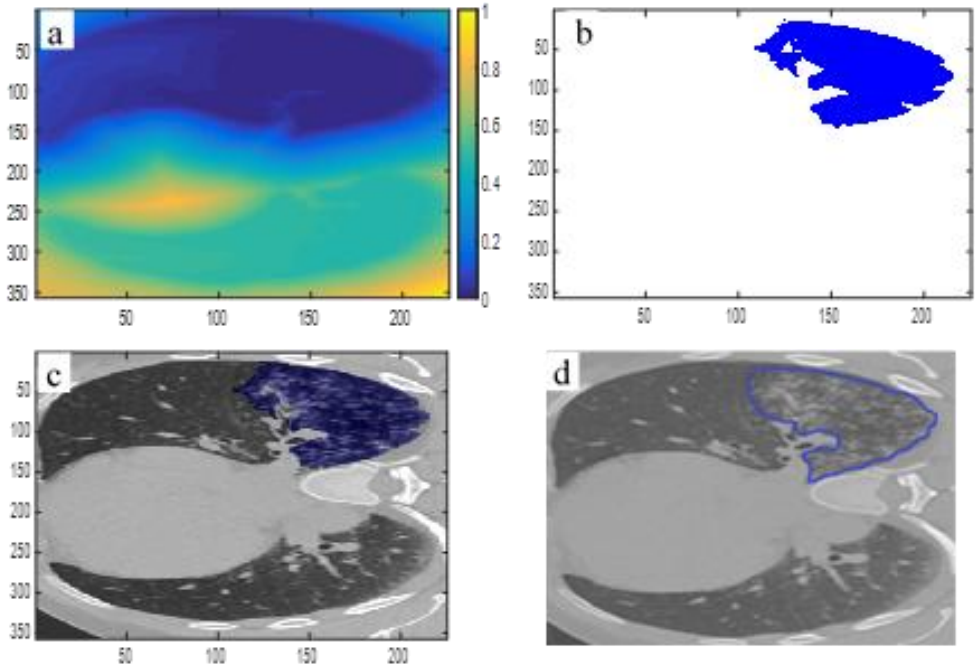

Fig. 5. (a) normalized geodesic distance map, (b) RGB segmented region of infection, (c) superimposed RGB image over CT grayscale lungs image, (d) physician delineated of infection region

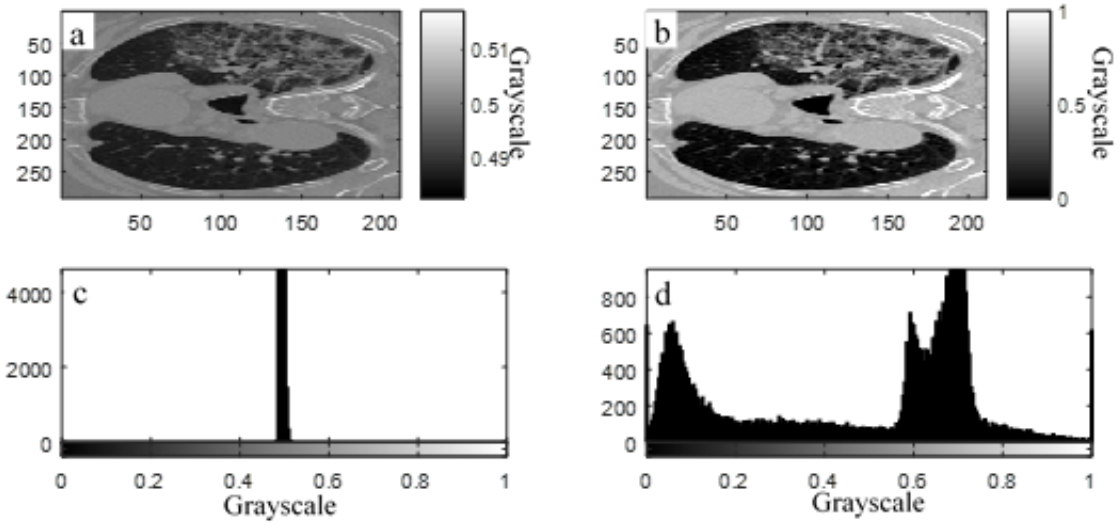

Fig. 6. Grayscale CT, (a) acquired image, (b) intensity adjusted image, (c) histogram of acquired image, (d) histogram of intensity adjusted image

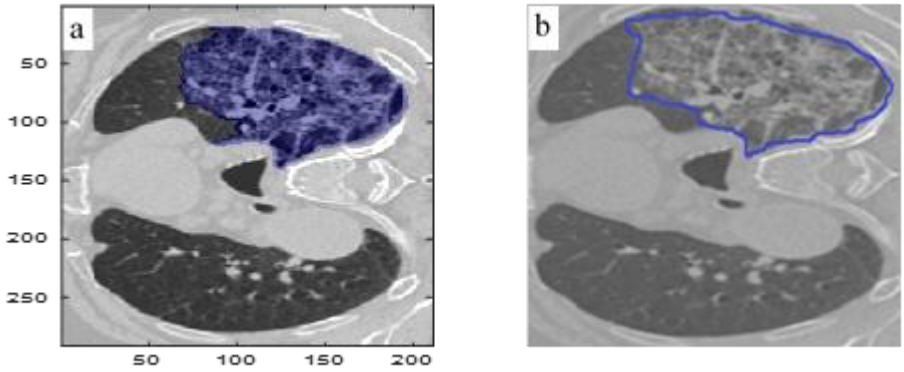

Fig. 7. (a) Algorithm segmentation, (b) physician delineation of infection region

5. Conclusion

In CT image, COVID infection of lungs occurred in ground glass fashion that challenge image segmentation techniques due to non-existence of edge and non-structuring object. The proposed algorithm introduced to facilitate these challenges by combining both morphological reconstruction and fast marching method. Results showed considerable determination of infection region that consistent with manual delineation of senior physician, where the performance of the proposed algorithm would be considered to reinforce the physician diagnoses efforts and reducing time consumption. Empirical determination of FMM's threshold has to be evaluated to surpass algorithm limitation. The proposed algorithm can also be conducted for segmentation of histopathology image region of interest. Further investigation would be considered for quantitative performance evaluation by including further patients from the dataset with the objective of considering adaptive threshold. Furthermore, three dimensional visualizations of COVID infection region has been targeted based on accumulation of 2D segmentation for physician conceive of lungs dysfunction.

Acknowledgment

The authors would like to express my special thanks of gratitude to the staff in the Department of Medical Techniques Engineering, College of Electrical Engineering Techniques, and Middle Technical University for their support to conduct this work.

Reference

[1] P. Rai, B. K. Kumar, V. K. Deekshit, I. Karunasagar, and I. Karunasagar, "Detection technologies and recent developments in the diagnosis of COVID-19 infection," Applied Microbiology and Biotechnology, pp. 1-15, 2021.
[2] D. Chen, X. Jiang, Y. Hong, Z. Wen, S. Wei, G. Peng, et al., "Can Chest CT Features Distinguish Patients With Negative From Those With Positive Initial RT-PCR Results for Coronavirus Disease (COVID-19)?," American Journal of Roentgenology, vol. 216, pp. 66-70, 2021/01/01 2020.
[3] F. Shi, J. Wang, J. Shi, Z. Wu, Q. Wang, Z. Tang, et al., "Review of artificial intelligence techniques in imaging data acquisition, segmentation, and diagnosis for COVID-19," IEEE reviews in biomedical engineering, vol. 14, pp. 4-15, 2020.
[4] M. Kim and B.-D. Lee, "Automatic lung segmentation on chest X-rays using self-attention deep neural network," Sensors, vol. 21, p. 369, 2021.
[5] T. Agrawal and P. Choudhary, "Segmentation and classification on chest radiography: a systematic survey," The Visual Computer, pp. 1-39, 2022.
[6] S. Pandey, P. R. Singh, and J. Tian, "An image augmentation approach using two-stage generative adversarial network for nuclei image segmentation," Biomedical Signal Processing and Control, vol. 57, p. 101782, 2020.
[7] S. T. H. Kieu, A. Bade, M. H. A. Hijazi, and H. Kolivand, "A Survey of Deep Learning for Lung Disease Detection on Medical Images: State-of-the-Art, Taxonomy, Issues and Future Directions," Journal of Imaging, vol. 6, p. 131, 2020.
[8] A. Oulefki, S. Agaian, T. Trongtirakul, S. Benbelkacem, D. Aouam, N. Zenati-Henda, et al., "Virtual Reality visualization for computerized COVID-19 lesion segmentation and interpretation," Biomedical Signal Processing and Control, vol. 73, p. 103371, 2022.
[9] D.-P. Fan, T. Zhou, G.-P. Ji, Y. Zhou, G. Chen, H. Fu, et al., "Inf-net: Automatic covid-19 lung infection segmentation from ct images," IEEE Transactions on Medical Imaging, vol. 39, pp. 2626-2637, 2020.
[10] X. Lei and H. Ouyang, "Image segmentation algorithm based on improved fuzzy clustering," Cluster Computing, vol. 22, pp. 13911-13921, 2019.
[11] S.-M. Hou, C.-L. Jia, M.-J. Hou, S. L. Fernandes, and J.-C. Guo, "A Study on Weak Edge Detection of COVID-19's CT Images Based on Histogram Equalization and Improved Canny Algorithm," Computational and Mathematical Methods in Medicine, vol. 2021, 2021.
[12] R. K. Kalia, A. Sharma, S. B. Amin, M. Saha, and S. K. Thittamaranahalli, "Ai-Driven Quantification Of Ground Glass Opacities In Lungs Of Covid-19 Patients Using 3d Computed Tomography Imaging," medRxiv, 2021.
[13] X. A. Inbaraj, C. Villavicencio, J. J. Macrohon, J.-H. Jeng, and J.-G. Hsieh, "A Novel Machine Learning Approach for Tuberculosis Segmentation and Prediction Using Chest-X-Ray (CXR) Images," Applied Sciences, vol. 11, p. 9057, 2021.
[14] S. Chakraborty and K. Mali, "SUFMACS: a machine learning-based robust image segmentation framework for covid-19 radiological image interpretation," Expert Systems with Applications, vol. 178, p. 115069, 2021.
[15] E. Jangam and A. Rao, "Segmentation of lungs from chest X rays using firefly optimized fuzzy C-means and level set algorithm," in

International Conference on Recent Trends in Image Processing and Pattern Recognition, 2018, pp. 303-311.
[16] J. Tan, L. Jing, Y. Huo, L. Li, O. Akin, and Y. Tian, "Lgan: Lung segmentation in ct scans using generative adversarial network," Computerized Medical Imaging and Graphics, vol. 87, p. 101817, 2021.
[17] S. Chakraborty and K. Mali, "SuFMoFPA: A superpixel and meta-heuristic based fuzzy image segmentation approach to explicate COVID-19 radiological images," Expert Systems with Applications, vol. 167, p. 114142, 2021.
[18] S. Chakraborty and K. Mali, "Fuzzy Electromagnetism Optimization (FEMO) and its application in biomedical image segmentation," Applied Soft Computing, vol. 97, p. 106800, 2020.
[19] A. M. Hasan, M. M. Al-Jawad, H. A. Jalab, H. Shaiba, R. W. Ibrahim, and A. a. R. AL-Shamasneh, "Classification of Covid-19 coronavirus, pneumonia and healthy lungs in CT scans using Q-deformed entropy and deep learning features," Entropy, vol. 22, p. 517, 2020.
[20] T. Zhou, S. Canu, and S. Ruan, "An automatic covid-19 ct segmentation based on u-net with attention mechanism," arXiv preprint arXiv:2004.06673, 2020.
[21] K. Gao, J. Su, Z. Jiang, L.-L. Zeng, Z. Feng, H. Shen, et al., "Dual-branch combination network (DCN): Towards accurate diagnosis and lesion segmentation of COVID-19 using CT images," Medical image analysis, vol. 67, p. 101836, 2021.
[22] M. Xu, S. Qi, Y. Yue, Y. Teng, L. Xu, Y. Yao, et al., "Segmentation of lung parenchyma in CT images using CNN trained with the clustering algorithm generated dataset," Biomedical engineering online, vol. 18, pp. 1-21, 2019.
[23] Y. A. Hamad, M. E. Seno, M. Al-Kubaisi, and A. N. Safonova, "Segmentation and measurement of lung pathological changes for COVID-19 diagnosis based on computed tomography," Periodicals of Engineering and Natural Sciences, vol. 9, pp. 29-41, 2021.
[24] N. Dhanachandra and Y. J. Chanu, "An image segmentation approach based on fuzzy c-means and dynamic particle swarm optimization algorithm," Multimedia Tools & Applications, vol. 79, 2020.
[25] K. Mardani and K. Maghooli, "Enhancing retinal blood vessel segmentation in medical images using combined segmentation modes extracted by DBSCAN and morphological reconstruction," Biomedical Signal Processing and Control, vol. 69, p. 102837, 2021.
[26] J.-W. Baek and K. Chung, "Pothole classification model using edge detection in road image," Applied Sciences, vol. 10, p. 6662, 2020.
[27] A. N. Mathew, J. M. Kuriakose, S. Haridas, and S. John, "Study on Alzheimer's disease using Image Processing," Journal of Embedded Systems and Processing, vol. 4.
[28] L. Vincent, "Morphological grayscale reconstruction in image analysis: applications and efficient algorithms," IEEE transactions on image processing, vol. 2, pp. 176-201, 1993.
[29] J. Serra, Image Analysis and Mathematical Morphology: Vol.: 2: Theoretical Advances: Academic Press, 1988.
[30] T. Lei, X. Jia, T. Liu, S. Liu, H. Meng, and A. K. Nandi, "Adaptive morphological reconstruction for seeded image segmentation," IEEE Transactions on Image Processing, vol. 28, pp. 5510-5523, 2019.
[31] R. D. Yapa and K. Harada, "Application of Fast-Marching method on mammograms for breast skin-line estimation," in 2007 International Conference on Industrial and Information Systems, 2007, pp. 59-62.
[32] K. Clark, B. Vendt, K. Smith, J. Freymann, J. Kirby, P. Koppel, et al., "The Cancer Imaging Archive (TCIA): maintaining and operating a public information repository," Journal of digital imaging, vol. 26, pp. 1045-1057, 2013.